

## Deep learning-derived splenic radiomics, genomics, and coronary artery disease

Meghana Kamineni (1), Vineet Raghv (2, 3), Buu Truong (4,5), Ahmed Alaa (6,7), Art Schuermans (4, 5, 8), Sam Friedman (9), Christopher Reeder (9), Romit Bhattacharya (10, 11), Peter Libby (12), Patrick T. Ellinor (4, 5, 13, 14), Mahnaz Maddah (9), Anthony Philippakis (15), Whitney Hornsby (4, 5), Zhi Yu\* (4, 5), Pradeep Natarajan\*(1,4,5,16)

\* These authors jointly supervised this work.

### Affiliations

1. Harvard Medical School, Boston, MA
2. Cardiovascular Imaging Research Center, Department of Radiology, MGH and HMS
3. Artificial Intelligence in Medicine Program, Mass General Brigham, Harvard Medical School, Boston, Massachusetts
4. Program in Medical and Population Genetics, Broad Institute of MIT and Harvard, Cambridge, MA
5. Center for Genomic Medicine and Cardiovascular Research Center, Massachusetts General Hospital, Boston, MA
6. Computational Precision Health Program, University of California, Berkeley, Berkeley, CA 94720
7. Computational Precision Health Program, University of California, San Francisco, San Francisco, CA 94143
8. Faculty of Medicine, KU Leuven, Leuven, Belgium
9. Data Sciences Platform, Broad Institute of MIT and Harvard, Cambridge, MA

10. Division of Cardiology, Massachusetts General Hospital, Harvard Medical School, 55 Fruit Street, Boston MA 02114

11. Cardiovascular Research Center, Massachusetts General Hospital, Boston, MA

12. Division of Cardiovascular Medicine, Brigham and Women's Hospital, Harvard Medical School, 77 Avenue Louis Pasteur, Boston, MA 02115

13. Cardiovascular Disease Initiative, Broad Institute of Harvard and MIT, Cambridge, MA, USA

14. Demoulas Center for Cardiac Arrhythmias, Massachusetts General Hospital, Boston, MA, USA

15. GV, Cambridge, MA

16. Personalized Medicine, Mass General Brigham, Boston, MA

Please address correspondence to:

Zhi Yu, MB, PhD

75 Ames Street, Cambridge, MA 02142

617-714-7223

[zyu@broadinstitute.org](mailto:zyu@broadinstitute.org)

Pradeep Natarajan, MD MMSc

185 Cambridge Street, CPZN 5.238, Boston, MA 02114

617-726-1843

[pnatarajan@mgh.harvard.edu](mailto:pnatarajan@mgh.harvard.edu)

1 **Abstract**

2 **Background:**

3 Despite advances in managing traditional risk factors, coronary artery disease (CAD) remains the  
4 leading cause of mortality. Circulating hematopoietic cells influence risk for CAD, but the role  
5 of a key regulating organ, spleen, is unknown. The understudied spleen is a 3-dimensional  
6 structure of the hematopoietic system optimally suited for unbiased radiologic investigations  
7 toward novel mechanistic insights.

8 **Methods:**

9 Deep learning-based image segmentation and radiomics techniques were utilized to extract  
10 splenic radiomic features from abdominal MRIs of 42,059 UK Biobank participants. Regression  
11 analysis was used to identify splenic radiomics features associated with CAD. Genome-wide  
12 association analyses were applied to identify loci associated with these radiomics features.  
13 Overlap between loci associated with CAD and the splenic radiomics features was explored to  
14 understand the underlying genetic mechanisms of the role of the spleen in CAD.

15 **Results:**

16 We extracted 107 splenic radiomics features from abdominal MRIs, and of these, 10 features  
17 were associated with CAD. Genome-wide association analysis of CAD-associated features  
18 identified 219 loci, including 35 previously reported CAD loci, 7 of which were not associated  
19 with conventional CAD risk factors. Notably, variants at 9p21 were associated with splenic  
20 features such as run length non-uniformity.

21 **Conclusions:**

22 Our study, combining deep learning with genomics, presents a new framework to uncover the  
23 splenic axis of CAD. Notably, our study provides evidence for the underlying genetic connection

24 between the spleen as a candidate causal tissue-type and CAD with insight into the mechanisms  
25 of 9p21, whose mechanism is still elusive despite its initial discovery in 2007. More broadly, our  
26 study provides a unique application of deep learning radiomics to non-invasively find  
27 associations between imaging, genetics, and clinical outcomes.

## 28 Introduction

29 Despite advances in the management of traditional risk factors, coronary artery disease (CAD)  
30 remains the leading cause of mortality and disability-adjusted life-years (DALYs) worldwide.<sup>1,2</sup>  
31 Advances in CAD prevention beyond targeting traditional risk factors continue to remain limited  
32 due to poor understanding and limited mechanistic frameworks of such distinct CAD pathways.

33 The hematopoietic system has long been known to contribute to CAD, largely through  
34 inflammatory cells in both atherogenesis and atherosclerotic cardiovascular disease events.<sup>3</sup>  
35 Inflammation markers, such as high-sensitivity C-reactive protein (hsCRP), are independently  
36 predictive of CAD risk. Among individuals with CAD and high hsCRP, a monoclonal antibody  
37 targeting interleukin (IL)-1B reduced the risk for recurrent CAD events but increased risk for  
38 serious infections.<sup>4</sup> While this trial validated the causal role of inflammatory cytokines for CAD,  
39 the optimal strategy to modulate hematopoietic cells and their products toward CAD risk  
40 reduction remains poorly understood.<sup>5</sup>

41 Longstanding circumstantial evidence has suggested involvement of the spleen, an  
42 extramedullary hematopoietic organ, in CAD.<sup>6</sup> U.S. veterans who underwent splenectomy for  
43 trauma during World War II had greater mortality due to CAD in long-term follow-up.<sup>7</sup> More  
44 recently, the spleen was described as an important reservoir for undifferentiated inflammatory  
45 myeloid cells that are mobilized in the context of myocardial ischemic injury infiltrating  
46 myocardium in murine models.<sup>8</sup> Myelopoiesis after splenic activation, including during  
47 myocardial infarction, further leads to atherosclerosis instability in mice.<sup>9</sup> Post-mortem human  
48 samples from varying times after myocardial infarction demonstrate splenic monocyte depletion  
49 early after myocardial infarction, invoking their mobilization early in the event.<sup>10</sup> (18)F-  
50 fluorodeoxyglucose ((18)FDG)-positron emission tomography among patients who sustained

51 acute coronary syndromes showed that increased splenic metabolic activity strongly predicted  
52 recurrence.<sup>11</sup> More recent human genome-wide association studies (GWAS) of CAD have  
53 implicated splenic gene regulation. Individual inflammatory genes, including *CCR5*, prioritized  
54 through this approach are strongly expressed in the spleen.<sup>12</sup> Among the top signals for CAD  
55 GWAS, splenic tissue is one of the top three tissues enriched for variants residing within strong  
56 enhancers and active promoters. However, there is limited understanding regarding the critical  
57 factors regulating splenic function in relation to CAD risk.

58         Advancements in machine learning applied to medical imaging offer new opportunities  
59 for unbiased, scalable detection and quantification of subtle alterations in internal organs,  
60 including the spleen, where specific circulating biomarkers may be unavailable. Deep learning  
61 enables large-scale automatic segmentation of organs in medical images, bypassing time-  
62 consuming manual segmentation. Radiomics, an emerging field, quantifies features extracted  
63 from these segmentations to offer non-invasive insights into underlying pathologies. These  
64 features encapsulate a variety of metrics, such as shape, size, and texture.<sup>13</sup> For the spleen,  
65 radiomics have been used to diagnose and differentiate lymphoma subtypes and predict the  
66 recurrence of hepatocellular carcinoma.<sup>14</sup> Radiomics offers an opportunity to glean novel  
67 insights about splenic anatomy as typically only splenic size is annotated in clinical scans.

68         In this study, we leveraged deep learning and radiomic analyses to extract and discover  
69 CAD-relevant splenic features from abdominal magnetic resonance imaging (MRI). Additionally  
70 using genomics, we further prioritize previously poorly known CAD-associated loci and genes  
71 with key splenic radiomic features. Utilizing a multi-disciplinary approach that integrates  
72 advanced imaging analyses, genomics, and clinical outcomes, our study introduces a new  
73 framework for understanding the spleen's potential role in residual CAD risk.

## 74 **Methods**

### 75 *Cohort selection and workflow*

76 The UK Biobank is a volunteer cohort of approximately 500,000 participants aged 40-69 years  
77 recruited from 2006 to 2010 with ongoing prospective follow-up.<sup>15</sup> At baseline, participants  
78 provided surveys, biospecimens, anthropometrics, vital signs, and other study-specific  
79 procedures. Approximately 50,000 MRIs were performed for a subset of participants after  
80 reinvitation beginning in 2014. We limited our study population to those who had abdominal  
81 MRIs acquired during the study and whose spleen and liver segments were identifiable after  
82 applying our segmentation algorithm. Analysis of the UK Biobank data was approved by the UK  
83 Biobank application 7089 and Massachusetts General Hospital IRB protocol 2021P002228. The  
84 inclusion and exclusion criteria are visualized in **Supplemental Figure 1**.

85 **Figure 1** illustrates the study workflow. First, we segmented the spleen from abdominal  
86 MRIs and extracted comprehensive radiomic features linked to intrinsic splenic properties. Next,  
87 we used regression models to discover independent splenic features associated with CAD, which  
88 we investigated in subsequent analyses. We then performed GWAS to identify genetic variants  
89 associated with each of the CAD-associated splenic phenotypes, building on which we (1)  
90 prioritized genes that are likely to be causal and probed their functional relevance to CAD and (2)  
91 identified overlapping genetic variants that are significantly associated with both splenic  
92 phenotypes and CAD, whose corresponding functions may be the link between the spleen and  
93 residual CAD risk.

94

### 95 *Phenotyping of clinical and demographic variables*

96 CAD was defined as a history of coronary artery bypass grafting, myocardial infarction (MI),  
97 coronary artery angioplasty, or billing codes (OPCS-4: K40, K41, K45, K49, K50.2, K75) as  
98 previously performed.<sup>16</sup> Prevalent and incident CAD status were defined by whether participants  
99 were diagnosed with CAD before or after the time of their MRI. Demographic variables were all  
100 ascertained at enrollment and included age, race, and sex of participants.

101

### 102 *Genotyping and genome-wide association study*

103 The genotyping procedures of the UK Biobank have been described previously in detail.<sup>15</sup> The  
104 genotyping arrays were the UK BiLEVE Axiom Array or the UK Biobank Axiom Array (both  
105 Affymetrix). The array-derived genotypes were imputed using the Haplotype Reference  
106 Consortium, UK10K, and 1000 Genome reference panels. Variant quality control measures  
107 included the following filters:  $MAF \geq 1\%$ , single nucleotide variant missingness  $< 10\%$  and HWE  
108  $P \geq 10^{-15}$ ,  $MAC \geq 50$ , and INFO score  $\geq 0.6$ . Sample quality control measures included  
109 excluding individuals if the single nucleotide variant missingness was equal to or exceeded 10%.  
110 Association analysis was performed in participants of European ancestry using REGENIE with  
111 adjustment for age, sex, and first ten PC of genetic ancestry.

112

### 113 *Extraction of splenic features*

114 Briefly, the UK Biobank abdominal MRI protocol was as follows.<sup>17</sup> The study aimed to image  
115 100,000 healthy UK participants aged between 40 and 69 years old. 1.5 T clinical MRI scanners  
116 were utilized (Magnetom Aera, Siemens Healthineers, Erlangen, Germany) to acquire whole-  
117 body T1-weighted dual echo gradient echo (GRE) sequences. The parameters were as follows:  
118 echo times (2.39/4.77 ms), pixel size ( $2.23 \times 2.23 \text{ mm}^2$ ), slice thickness (3–4.5 mm), repetition



119 time (6.69 ms), and flip angle (10°). For each patient, four MRI contrasts were available: in-  
120 phase (IP), out-of-phase (OP), water, and fat. We downloaded all abdominal MRIs from the UK  
121 Biobank.

122 We then used deep learning to segment spleens from abdominal MRIs of our study  
123 population and extracted 107 splenic radiomic features. Briefly, we used a stitching algorithm to  
124 stitch together MRI scans from six acquisition stations and compose whole-body scans outputted  
125 as four phases: water, fat, in phase, and out of phase (<https://github.com/biomediamira/stitching>).<sup>34</sup> Utilizing a pre-trained nnuNet segmentation model, originally trained on  
126 10,000 UK Biobank abdominal MRIs, we generated predictions of voxels corresponding to the  
127 spleen (code: <https://github.com/BioMedIA/UKBB-GNC-Abdominal-Segmentation>, trained  
128 models: <https://gitlab.com/turkaykart/ukbb-gnc-abdominal-segmentation>).<sup>18</sup> This model had no  
129 errors in over 95% of the spleen segmentations in the UK Biobank data, and we performed no  
130 additional training. The models utilize a nnU-net architecture, a variant of the popular U-Net  
131 architecture that was shown to outperform U-Net on a range of biomedical imaging segmentation  
132 tasks. The models were validated in a previous study using 400 previously labeled images.<sup>18</sup> The  
133 inputs to the model were water, fat, in- and opposed-phase stitched MRs. The model was  
134 applied on a Google Cloud Platform with CUDA version 11.6 and with 2 Tesla T4 GPUs  
135 available with 16 GB RAM each. Lastly, we extracted the voxels that corresponded to the spleen  
136 segment.

137  
138 We applied the *pyradiomics* software (version 3.1.0) to the voxels identified by the model  
139 as spleen segments to extract shape and texture-based features.<sup>21</sup> Generation of these features  
140 includes first-order statistics describing the image region and computation of the relationships  
141 between neighboring pixels. All code was parallelized using multi-processing to decrease

142 runtime. In addition to the features extracted through this approach, we utilized the splenic  
143 volume features provided by the UK Biobank, which was determined using a deep learning U-  
144 net architecture as described in this study.<sup>22</sup>

145

#### 146 *Correlation of splenic features with each other and cardiometabolic outcomes*

147 We examined the associations of splenic features with age, sex, and BMI

148 (<https://biobank.ctsu.ox.ac.uk/showcase/field.cgi?id=21001>). We used a linear regression model

149 with each splenic feature as the independent variable and age at enrollment, sex, BMI, and days

150 between enrollment and MRI acquisition as dependent variables. All splenic radiomic features

151 were normalized to a distribution with mean 0 and standard deviation 1 for all analyses. We

152 reported the coefficients and standard errors of both BMI and sex for each splenic feature.

153 We also associated the splenic features with blood-based biomarkers available in the UK

154 Biobank. Blood-based markers include counts and percentages of basophils, eosinophils,

155 lymphocytes, monocytes, neutrophils, platelets, reticulocytes, high light scatter reticulocytes,

156 white blood cells, red blood cells, and nucleated red blood cells. Other biomarkers were C

157 reactive protein, hematocrit, hemoglobin concentration, immature reticulocyte fraction, mean

158 corpuscular hemoglobin, mean corpuscular hemoglobin concentration, mean corpuscular,

159 platelet, reticulocyte, and sphered cell volumes, and platelet and erythrocyte distribution width

160 (<https://biobank.ndph.ox.ac.uk/ukb/label.cgi?id=9081>). For each of the blood-based biomarkers,

161 we implemented a linear regression model with each splenic feature as the outcome and the

162 biomarker as a covariate and adjusted for age, sex, BMI, and the days between enrollment and

163 the MRI acquisition. We then reported the coefficient, which can be interpreted as the change in

164 one unit of the biomarker per 1 SD of the radiomic feature, and standard error of the biomarker  
165 in the model.

166

### 167 *Identification of splenic features associated with CAD*

168 We examined for splenic radiomic features that are associated with CAD outcomes. We  
169 differentiate between CAD diagnosed prior to MRI (prevalent cases) for assessing splenic  
170 markers of existing CAD, and first CAD after MRI (incident cases among those without  
171 prevalent CAD) for assessing splenic predictors of future CAD. We performed feature  
172 processing before training two models for the outcomes of prevalent and incident CAD. Race  
173 and sex were coded as binary indicator variables. For each feature, we imputed any missing  
174 values with the median of all values for the feature, since missingness was less than 10%. We  
175 then employed forward selection to identify independent features for each CAD outcome,  
176 thereby minimizing potential collinearity. Starting with all features including splenic features,  
177 age, race, and sex, this method selected features one at a time that had a P value of less than a  
178 threshold when added to a model with already included features  
179 (<https://github.com/AakkashVijayakumar/stepwise-regression/tree/master>). We selected this  
180 threshold using 5-fold cross-validation on a held-out validation set, and our threshold options  
181 were 0.025, 0.05, 0.1, and 0.2. After a subset of features was selected, we standardized all  
182 features to normal distributions.

183 Subsequently, we analyzed the associations between the selected radiomic features and  
184 CAD outcomes using L1-regularized multivariable regression models, specifically logistic  
185 regression and Cox proportional hazards for prevalent and incident CAD respectively. For each  
186 model, 70% and 30% of the data were utilized for training and evaluation respectively. To

187 identify splenic features associated with prevalent CAD, we trained an L1-regularized logistic  
188 regression model for the outcome of prevalent CAD. We optimized the logistic regression model  
189 using a 5-fold cross-validation grid search for various hyperparameters, including different  
190 regularization parameters ( $C = [5 \times 10^{-5}, 5 \times 10^{-4}, 5 \times 10^{-3}, 0.05, 0.5, 1, 5, 10]$ ), maximum number  
191 of training iterations ( $\text{max\_iter} = [1000, 5000]$ ), and reweighting of data points to minimize class  
192 imbalance ( $\text{class\_weight} = [\text{balanced}, \text{None}]$ ). We computed AUROC to evaluate the logistic  
193 regression. For the outcome of incident CAD, we used a Cox proportional hazards model in  
194 order to account for the temporal information of time from MRI acquisition to CAD diagnosis.  
195 The time event was the days from MRI date to CAD diagnosis, and patients with CAD diagnosis  
196 before MRI date were excluded from the analysis. We computed concordance and AIC to  
197 evaluate the model. To ascertain the robustness of our findings, we performed 1000 resamplings  
198 using Monte Carlo bootstrapping on the test set to calculate 95% CI of the AUROC or  
199 concordance index.

200

### 201 *Genome-wide association study and gene prioritization*

202 We explored the genetic underpinnings of CAD-associated splenic features by conducting  
203 GWAS on common variants (minor allele frequency  $> 0.01$ ) for the fourteen splenic radiomic  
204 features. We used the PLINK (version 2.0) and REGENIE (version 3.2.8) software to run a  
205 GWAS for each splenic feature for chromosomes 1-22. We used a minor allele frequency of 0.01,  
206 missingness upper threshold of 0.1, and Hardy-Weinberg equilibrium value of  $1 \times 10^{-15}$ . We  
207 adjusted for age, sex, first ten genetic PCs, and genotyping array. For all phenotypes, we  
208 computed the genomic inflation factor and the LD score intercept using LD Score Regression  
209 (LDSC) using LD scores from participants of European ancestry from the hapmap3 variants.<sup>23</sup>

210 To further analyze the results, we used the Functional Mapping and Annotation of  
211 Genome-Wide Studies (FUMA), a platform for annotation of GWAS results and gene  
212 prioritization.<sup>24</sup> Independent, significant loci were detected based on a significance threshold of  $p$   
213  $< 5 \times 10^{-8}$  and clumping with 1000 Genomes data, with an  $R^2$  threshold of 0.6. Lead SNPs were  
214 then detected based on clumping on independent, significant loci with an  $R^2$  threshold of 0.1. We  
215 used an online list comparator to identify overlapping lead SNPs  
216 (<https://molbiotools.com/listcompare.php>). For gene prioritization, we used FUMA to identify  
217 the nearest genes to each SNP and the genes prioritized by expression quantitative trait loci  
218 (eQTL).<sup>24</sup> The nearest gene to each SNP was identified using a window of 10 Kb of the SNP. We  
219 combined the PoPS analysis with positional mapping in order to prioritize genes, as combining  
220 similarity-based and locus-based approaches has been shown to lead to better identification of  
221 causal genes.<sup>25</sup> To implement PoPS, we first computed MAGMA scores from the summary-level  
222 results of the GWAS with each splenic feature. We then computed a PoPS score for all genes  
223 within 10 Kb of the significant SNPs. We selected the gene with the highest PoPS score in each  
224 locus. All GTEx v7 eQTL data were used for eQTL mapping, specifically adipose tissue, adrenal  
225 gland, blood, blood vessel, brain, breast, colon, esophagus, heart, liver, lung, muscle, nerve,  
226 ovary, pancreas, pituitary, pancreas, salivary gland, skin, small intestine, spleen, stomach, testis,  
227 thyroid, uterus, and vagina tissues. In order to prioritize genes using PoPS, we processed publicly  
228 available features derived from gene expression data from various organs  
229 ([https://github.com/FinucaneLab/gene\\_features](https://github.com/FinucaneLab/gene_features)). For the GWAS results for each splenic  
230 phenotype, we then applied MAGMA, which provides gene-level association statistics. Finally,  
231 we applied the PoPS algorithm to derive scores for each gene.<sup>26</sup> We stratified the genes by  
232 genomic locus and prioritized the gene with the highest PoPS score. For each splenic phenotype,

233 we filtered genes prioritized by at least two of the three methods. We then compiled all genes  
234 prioritized in this manner for any of the ten splenic phenotypes.

235 From the genes prioritized for the splenic phenotypes, we used OpenTargets to identify  
236 genes associated with CAD. Associations with CAD are based on a combination of scores based  
237 on data from Open Targets Genetics, ClinVar, an NIH public archive of the relationship between  
238 human genetic variants and phenotypes, and other genetic sources ([https://platform-](https://platform-docs.opentargets.org/evidence#open-targets-genetics)  
239 [docs.opentargets.org/evidence#open-targets-genetics](https://platform-docs.opentargets.org/evidence#open-targets-genetics)). We included all genes as associated with  
240 CAD if the overall association was greater than 0. For the genes with non-zero associations with  
241 CAD, we then searched for the mouse phenotypes in mice where the gene was knocked out using  
242 the International Mouse Phenotyping Consortium, a collaboration between 21 research  
243 institutions where approximately 20,000 genes are systemically knocked out one by one in mice  
244 to understand the resulting phenotypes.<sup>27,28</sup>

245

#### 246 *Overlap of SNPs and genetic correlation between splenic phenotypes and CAD*

247 We used GWAS results from a previous meta analysis for CAD for determining overlap and to  
248 identify genetic correlation.<sup>29</sup> We identified SNPs that were significantly associated with both  
249 CAD and at least one of the six splenic phenotypes. We used a p-value threshold of  $<5 \times 10^{-8}$  to  
250 define significant SNPs for both the CAD and splenic phenotype GWAS results. For each  
251 splenic phenotype, we clumped the significant SNPs overlapping with CAD using 1000  
252 Genomes reference panel of European participants to identify lead SNPs.<sup>23,30</sup> After filtering to  
253 SNPs meeting the genome-wide significance threshold, clumping of SNPs was performed using  
254 the default settings of 0.0001 as the significance threshold for index SNPs, 0.01 as the threshold  
255 for clumped SNPs, 0.50 as the LD threshold, 250 kb as the distance threshold, and 1000

256 Genomes patient cohort as the reference population. Next, we investigated the phenotype  
257 associations of the lead SNPs using PhenoScanner, a database that contains over 65 billion  
258 phenotype associations and 150 million unique variants.<sup>31,32</sup> To compute genetic correlation, we  
259 used existing heritability estimation software and 1000 Genomes European LD score data.<sup>23,30,33</sup>

260

## 261 **Results**

### 262 *Study population*

263 Our study included 42,059 participants in the UK Biobank study who had abdominal MRIs  
264 without known hematological cancer at the time of MRI (**Supplemental Figure 1**). The study  
265 population at enrollment had a mean age of 55.1 years (standard deviation [SD] 7.5), body-mass  
266 index (BMI) of 26.1 kg/m<sup>2</sup> (SD 4.2), comprised 52.1% females (N=21,895), and was  
267 predominantly of British White ancestry by self-report (96.7%, N=40,675). At MRI  
268 ascertainment, the prevalence of CAD, hypertension, hyperlipidemia, and type 2 diabetes was  
269 4.7% (N=1,987), 24.0% (N=10,082), 16.7% (N=7,010), and 3.0% (N=1,243), respectively. The  
270 median time from UK Biobank enrollment to MRI was 9.4 years [IQR: 6.8-12.0], and the  
271 median follow-up time after MRI was 5.00 years [IQR: 3.85-6.63]. Key hematologic parameters  
272 measured at enrollment showed a mean white blood cell count of  $6.6 \times 10^9$  cells/L (SD: 1.6),  
273 hemoglobin concentration of 14.2 g/dL (SD: 1.2), platelet count of  $249.9 \times 10^9$  cells/L (SD: 56.3),  
274 and hsCRP levels at 2.1 mg/L (SD: 3.6) (**Table 1**).

275

### 276 *Deep learning-extracted radiomic characteristics of the spleen*

277 In our study population, splenic volume was previously annotated by the UK Biobank centrally  
278 for 15,215 participants with a mean of 0.17 liters (SD 0.07). Splenic volume varied with age and  
279 sex. It decreased modestly with age in this middle-aged cohort, from 0.18 mg/g (SD: 0.07)  
280 among individuals aged 40-48 years to 0.16 mg/g (SD: 0.07) among those aged 62-70 years.  
281 Splenic volumes on average were lower in women (mean 0.14 mg/g, SD 0.05) compared to men  
282 (mean 0.19 mg/g, SD 0.07).

283 We generated spleen images from the first MRI for all 42,059 participants. We extracted  
284 107 radiomic features using the pyradiomics software (version 3.0.1).<sup>21</sup> Features are grouped into  
285 first order statistics, 3D shape-based features, and five categories of gray level information  
286 (**Figure 2** and **Supplemental Table 1**).

287 We extracted 18 first-order statistics that indicate the distribution of voxel intensities  
288 within the masks of the image region. These features capture the magnitude, randomness,  
289 uniformity, and asymmetry of the voxel values, as well as standard descriptors such as mean,  
290 median, and range.

291 We derived 14 shape-based 3D metrics gleaned from the approximated shape defined by  
292 the triangle mesh independent of gray-level intensities using a ‘marching cubes’ algorithm.<sup>35</sup>  
293 These features are readily interpretable. As expected, several volume-related features, including  
294 mesh volume, voxel volume, major and minor axis lengths, and surface area are highly  
295 correlated with the annotated volume which was measured by the UK Biobank as part of the  
296 imaging exam (Pearson correlation coefficients [ $\rho$ ] ranging from 0.70 to 0.99; all  $P < 0.001$ ). In  
297 contrast, morphologic measures such as sphericity, elongation, and flatness exhibited relatively  
298 lower or no correlation with the annotated volume ( $\rho < 0.25$ ), indicating their orthogonal  
299 informational value (**Supplemental Table 2**).



300           The remaining 75 features focused on texture metrics relating to gray levels. We  
301 extracted gray level co-occurrence matrix (GLCM) to measure pixel intensity pairings within a  
302 spatial context, the gray level size zone matrix (GLSZM) to count interconnected voxels zones of  
303 similar grayness, and the gray level run length matrix (GLRLM) to assess the spatial  
304 distributions of these zones, reflecting graininess. 16 features were generated using each of these  
305 matrices. The neighboring gray tone difference matrix (NGTDM) estimates the variations in gray  
306 value over a specified distance for 5 features, and the gray level dependence matrix (GLDM)  
307 gauges the connectivity of voxels relative to a center voxel across 14 features. **Supplemental**  
308 **Figure 2** shows Pearson correlation coefficients between features, and further details are in  
309 <https://pyradiomics.readthedocs.io/en/latest/features.html> and **Supplemental Table 1**.

310

### 311 *Splenic radiomics with other variables*

312           Given the known influences of age, sex, and obesity on splenic function, we examined  
313 the association of age, sex, and BMI (after adjustment for the others) with each splenic feature  
314 using multivariable linear regression and observed many significant associations. In particular,  
315 sex showed the strongest associations with splenic size including minor axis length (0.7 SD  
316 lower in females vs males, 95% CI [0.68,0.72]) and surface area (0.70 [0.68,0.72]). BMI was  
317 most significantly associated with several texture features: one unit increase in BMI was  
318 associated with 0.11 [95% CI: 0.10, 0.11], 0.09 [0.09, 0.10], 0.09 [0.09, 0.09] SD increase in  
319 GLSZM gray level non-uniformity, run length non-uniformity, and GLRLM gray level non-  
320 uniformity, respectively (**Figure 3** and **Supplemental Figure 3**).

321           We then examined the associations between splenic features and hematologic biomarkers,  
322 adjusting for age, sex, and BMI. The strongest associations were of energy and GLSZM size

323 zone non-uniformity exhibited with high light scatter reticulocyte count, with an increase of 0.21  
324 [95% CI: 0.21, 0.21] per 1 SD of each radiomics feature. Many splenic features were negatively  
325 associated with mean spherical cell volume, including surface area (**Supplemental Figure 4**).  
326 The strongest association for white blood cell (WBC) count was a 0.10 [0.09, 0.11] increase for 1  
327 SD increase of GLCM informational measure of correlation 1. For red blood cell count, a 0.16  
328 [0.15, 0.17] increase was associated with 1 SD increase of GLSZM size zone non-uniformity.  
329 For C-reactive protein, a 0.05 [0.03, 0.06] increase was associated with 1 SD increase of median.  
330 **Supplemental Table 3** contains the top splenic radiomic features associated with each  
331 hematological parameter.

332

### 333 *Prioritizing CAD-associated splenic radiomics*

334 For prevalent CAD, the optimized regression model achieved an AUROC of 0.77 (95%  
335 CI 0.75-0.78) in the held-out test set (N=12755), and the Cox model for incident CAD yielded a  
336 concordance index of 0.68 (95% CI 0.65-0.71) in the test set (N=12022). Notably, 9 and 5  
337 splenic radiomic features were retained in the prevalent and incident CAD models, respectively,  
338 achieving statistical significance ( $P < 0.05$ ) after adjustment for other covariates.<sup>36</sup> There is no  
339 overlap in significant splenic features between prevalent and incident CAD. For prevalent CAD,  
340 associated features included GLSZM gray level non-uniformity (OR per 1 SD increase: 1.59 [95%  
341 CI: 1.38, 1.82],  $P < 0.001$ , FDR < 0.001) and sphericity (OR: 1.16 [95% CI: 1.09, 1.23],  $P < 0.001$ ,  
342 FDR < 0.001), among others. GLCM correlation, energy, GLDM metrics of small dependence  
343 high gray level emphasis and gray level variance, GLSZM large area low gray level emphasis,  
344 GLRLM run length non-uniformity, and GLCM inverse difference also showed significant  
345 associations with prevalent CAD. For incident CAD, associated features included GLRLM run

346 length non-uniformity (HR: 1.17 [95% CI: 1.09, 1.25], FDR<0.001), which was also associated  
347 with prevalent CAD, and GLCM inverse difference normalized (HR: 0.90 [95% CI: 0.85, 0.95],  
348 FDR<0.001) (**Supplemental Table 4, Figure 4A-B**). All features significantly associated with  
349 prevalent or incident CAD met the FDR threshold of 0.05 for significance for genetic discovery  
350 and were used for subsequent analyses.

351 To examine the relationships between these CAD-associated splenic features and  
352 conventional CAD risk factors, including age, sex, race, smoking, BMI, diabetes, hypertension,  
353 and total, HDL, and LDL cholesterol levels, we calculated their pairwise Pearson correlations.  
354 Gray level-uniformity, energy, and run-length non-uniformity are moderately positively  
355 correlated with BMI and triglyceride levels, and all three features negatively correlate with HDL  
356 cholesterol. Overall, most features exhibit only weak correlations with all conventional CAD risk  
357 factors (**Figure 4C**). **Supplemental Figure 5** shows representative MRI images for the  
358 prioritized splenic features.

359

### 360 *219 genome-wide significant regions associated with CAD-associated splenic features*

361 In the GWAS for the fourteen splenic radiomics features, there was no significant inflation of  
362 association statistics ( $\lambda_{GC}$  ranges from 1.03 to 1.15; LD score intercept ranges from 1.03 to 1.17.  
363 **Supplemental Table 5**). The genetic signals varied across the 14 traits. Using  $P < 5 \times 10^{-8}$  and  $r^2$   
364  $< 0.1$  as thresholds to identify significant and independent variants, we discovered 95  
365 independent significant SNPs for sphericity, 72 for energy, 41 for GLRLM run length non-  
366 uniformity, 21 for GLSZM gray level non-uniformity, and 16, 9, 7, 4, 2, and 0 for GLSZM large  
367 area low gray level emphasis, GLCM inverse difference, GLCM inverse difference normalized,  
368 GLCM correlation, GLDM small dependence high gray level emphasis, and GLDM gray level

369 variance, respectively. At the locus level, chr9:91392686, chr12:112037450, chr12:112007756,  
370 and 12:113165247 were all associated with 4 splenic features respectively; a few other  
371 discovered loci also associated with more than one feature, but more were associated with unique  
372 traits (**Figure 5, Supplemental Figures 6-14**).

373 Utilizing GWAS results of CAD-associated splenic features, we assessed their genetic  
374 correlations with CAD, observing varying degrees of correlations. The features with the  
375 strongest correlations that had the same direction of effect on CAD as in the regression models  
376 were GLCM correlation ( $r_g=0.17$ ,  $P=0.002$ ) and energy ( $r_g=-0.12$ ,  $P=0.01$ ), indicating shared  
377 genetic basis with CAD. A few features had more modest genetic correlations with CAD,  
378 suggesting the need for studying the non-genetic pathways linking them with CAD  
379 (**Supplemental Table 15**).

380  
381 *THBS1, PDE5A, and 35 more CAD-associated genes are likely to be causal genes for splenic*  
382 *features*

383 For GWAS of each CAD-associated splenic feature, we prioritized genes likely to be causal  
384 using three methods: 1) gene annotation based on distance (i.e., nearest gene), 2) polygenic  
385 priority score (PoPS), and 3) eQTL mapping based on cis-eQTLs. These loci mapped to 83, 58,  
386 35, 21, 16, 9, 7, 4, 2, 0 respective genes based on proximity, by choosing the closest gene to each  
387 SNP within 10 Kb, for the splenic phenotypes listed in the order from the previous section  
388 (**Supplemental Tables 6-14**). The strongest signals for sphericity and GLDM small dependence  
389 high gray level emphasis were annotated to *TLX1NB* and *LRRC37A2:ARL17A*, and the signals  
390 for the other features were near *ATXN2*, a multi-functional gene linked to circadian rhythm and  
391 neurodegenerative diseases and prioritized in a previous GWAS for splenic volume.<sup>22,37</sup>

392 Using PoPS, we prioritized 0 to 48 genes per feature, with top putative causal genes  
393 including *SIPR3*, *ARHGAP42*, *SMG6*,<sup>38</sup> *IRS1*, and *THBS1*, which were prioritized for 3 or more  
394 splenic features. *SIPR3* encodes a lysophospholipid mediator that has been shown to have both  
395 protective effects against stroke and vasoconstrictor effects.<sup>39</sup> We observed strong corroboration  
396 between prioritized genes by PoPS (similarity-based approach) and distance (locus-based),  
397 increasing confidence in the results (**Supplemental Tables 16-24**).<sup>26</sup> Using eQTL data from  
398 GTEx v7,<sup>40</sup> top genes prioritized by eQTL mapping prioritized include *SIPR3*, *EGF*, *HECTD4*,  
399 *ARHGAP42*, *NAA25*, and *SMG6*, which were all prioritized for at least 4 splenic features, and are  
400 similar to those prioritized by nearest genes and PoPS (**Supplemental Tables 16-24**).  
401 Collectively, 119 genes were prioritized by at least two gene prioritization methods across all  
402 phenotypes (**Supplemental Table 25** and **Figure 6**).

403 We explored the functional implications of genes prioritized for their links to CAD,  
404 leveraging OpenTargets to assess their CAD associations and the availability of targeted  
405 therapies. Among these, 37 genes, including *EGF*, *HECTD4*, *ARHGAP42*, *NAA25*, *SMG6*, *RPL6*,  
406 *IRS1*, *THBS1*, *PDE5A*, *FTTO*, *PPARG*, *CUX2*, have established CAD associations based on  
407 various genetic data sources (**Supplemental Table 25, Methods**).<sup>31,32</sup> These genes are involved  
408 in multiple mechanisms, including inflammation (e.g., *THBS1*), smooth muscle cell regulation  
409 (e.g., *TCF21*, *PDE5A*), hypertension (e.g., *HECTD4*, *ARHGAP42*), heart tissue development  
410 (e.g., *WNT5A*, *HAND2*, *TCF21*), and adipogenesis (e.g., *FTO*, *PPARG*). We traced back the 37  
411 genes to our GWAS across splenic features and found many were discovered from energy, run-  
412 length non-uniformity, and sphericity GWAS (**Supplemental Table 25**). For each gene, we  
413 identified mouse phenotypes resulting from gene knockout using the International Mouse  
414 Phenotyping Consortium.<sup>27,28</sup> Knocking out *SMG6*, *PDE5A*, and *TCF21* resulted in abnormal

415 spleen morphology, enlarged spleens for *SMG6* and *PDE5A*, and small spleens for *TCF21*.

416 *TCF21* knockout led to abnormal blood vessels. *THBS1* knockout led to abnormal and enlarged  
417 hearts (**Supplemental Table 25**).

418

419 *Overlap of SNPs and genetic correlation shed light on the link between splenic phenotypes and*  
420 *CAD*

421 Utilizing previously published CAD GWAS,<sup>29</sup> we compiled SNPs associated with CAD and  
422 identified the ones associated with splenic features. 396 and 390 CAD-associated SNPs were  
423 associated with energy and run-length non-uniformity respectively, and the overall median [IQR]  
424 number of SNPs associated with CAD and the splenic features was 255.5 [18, 337]. After  
425 clumping of SNPs, 24 and 22 independent CAD-associated SNPs were significantly associated  
426 with energy and run-length non-uniformity, respectively. The overall median [IQR] number of  
427 SNPs associated with CAD and the splenic features was 9 [3, 17], with 39 unique ones across all  
428 splenic phenotypes (**Supplemental Table 26**). We filtered to 35 lead SNPs where the effect  
429 direction of the SNP on CAD was consistent with the effect of at least one radiomic feature on  
430 CAD risk.

431 We interrogated the existing associations of lead SNPs using PhenoScanner<sup>31,32</sup> to assess  
432 for pleiotropic associations (**Supplemental Table 27**). Of the 35 SNPs, 7 (20%) were not  
433 associated with any known cardiovascular risk factor, including hypertension, diabetes, systolic  
434 and diastolic blood pressure, smoking, total, HDL, and LDL cholesterol, triglycerides, or weight  
435 (**Supplemental Figure 15**). These SNPs were rs7036656 (chr9p21.3), rs56750693  
436 (chr12q24.12), rs11515 (chr9p21.3), rs4239427 (chr18q11.2), rs4098854 (chr12q24.12),  
437 rs1208250 (chr6q23.2), and rs1208258 (chr6q23.2). These SNPs were associated with GLSZM

438 gray non-uniformity, energy, GLSZM large area low gray level emphasis, GLRLM run length  
439 non-uniformity, GLCM inverse difference, sphericity, and GLDM large dependence high gray  
440 level emphasis.

441 The top SNPs at two identified loci, rs7036656 and rs11515, are at the chr9p21 locus, the  
442 most strongly associated CAD locus but previously with limited mechanistic insight.<sup>41</sup> The  
443 rs7036656 SNP is significantly associated with energy ( $P=1.5\times 10^{-20}$ ), GLRLM run length non-  
444 uniformity ( $P=1.6\times 10^{-16}$ ), GLSZM large area low gray level emphasis ( $P=8.0\times 10^{-9}$ ), GLSZM  
445 gray non-uniformity ( $P=3.4\times 10^{-9}$ ), and GLCM inverse difference ( $P=3.2\times 10^{-8}$ ). The rs11515  
446 SNP is significantly associated with energy ( $P=2.4\times 10^{-11}$ ) and run length non-uniformity  
447 ( $P=3.3\times 10^{-9}$ ). Both loci are associated with energy and run-length non-uniformity. The strongest  
448 signal in the GWAS for both energy and run-length non-uniformity was at the same locus,  
449 rs653178 (energy:  $P = 1.3\times 10^{-106}$ , Z score = 21.9; run\_length non-uniformity:  $P = 9.2\times 10^{-72}$ , Z  
450 score = 17.9; nearest gene: *ATXN2*), indicating further genetic overlap between the two  
451 radiomics features. This locus is associated with systolic and diastolic blood pressure.<sup>42</sup>

## 452 Discussion

453 In this study, we harnessed deep learning to extract splenic phenotypes not readily quantifiable  
454 through conventional methods, establishing the link between spleen and CAD. We discovered  
455 several radiomic features, such as heightened sphericity, increased texture variation, and reduced  
456 gray level intensity in the spleen, that were robustly associated with elevated CAD risk. We  
457 explored the genetic underpinnings of these CAD-associated splenic features, providing insight  
458 into the potential mechanism of the spleen's involvement in key processes related to CAD, such  
459 as inflammation, smooth muscle cell regulation, and hypertension. Notably, we mapped seven

460 genetic loci unlinked to known CAD risk factors to the splenic features, offering potential new  
461 targets for intervention and dissecting the splenic axis of CAD.

462 Our study has several implications. The first is that novel deep learning techniques to  
463 non-invasively extract radiomic features in the spleen at scale enable association study and  
464 genomic analysis of splenic variation in the population. This approach is particularly pertinent  
465 for the spleen, an organ with limited annotations even in clinical reports. Furthermore, in our  
466 study, the splenic radiomic features carry detailed information on shape, size, texture, and  
467 intensity much beyond known splenic markers - except for volume-related splenic features  
468 highly correlated with known splenic volume, other features provided orthogonal information  
469 about the spleen. Lastly, the pipeline we built offers a scalable framework for extracting features  
470 of other organs from imaging, facilitating the construction and testing of novel biomedical  
471 hypotheses.

472 Second, we put the computer-learned features in a disease context and identified potential  
473 radiomic markers for CAD. For example, image-derived texture variation has been used to  
474 identify specific patterns within lymphoma, splenic infarction, and splenic cysts<sup>43</sup>; specific to  
475 splenic features, sphericity and flatness have previously been used to distinguish between  
476 lymphoma subtypes.<sup>14</sup> Our work expanded their use to look across all splenic radiomic features,  
477 capturing several aspects of spleen, and comprehensively examined the potential markers of  
478 CAD. We also identified splenic features common to patients both before and after CAD  
479 diagnosis, specifically run-length non-uniformity, suggesting that increases in splenic texture  
480 variation occur before CAD diagnosis and persist after diagnosis. This finding provides evidence  
481 that splenic changes are present with early development of CAD and are not simply effects of  
482 later disease progression.



483 Third, we integrated genetics and yielded important discoveries on the potential  
484 mechanism linking the spleen to CAD. Through GWAS and subsequent gene prioritization and  
485 annotation, we identified causal genes of CAD-associated splenic features and found their strong  
486 relevance in inflammation, smooth muscle cell regulation, and hypertension. For example, a top  
487 prioritized gene *THBS1* is implicated in angiogenesis and inflammation; *PDE5A*, essential for  
488 smooth muscle cell relaxation and linked to CAD through dysfunctional nitric oxide signaling  
489 and the second messenger cGMP in atherosclerosis, and *TCF21*, a regulator of coronary artery  
490 smooth muscle cell precursors, were prioritized.<sup>44,45,46</sup> Both *PDE5A* and *TCF21* knockouts in  
491 mice affect gross spleen morphology, highlighting their relevance to both CAD and splenic  
492 phenotypes and thus the validity of our findings.

493 Also, we identified 35 pleiotropic loci associated with CAD and splenic features, where  
494 the effect of the locus on the radiomics feature and CAD was consistent. Among them, 7 were  
495 not linked to any conventional CAD risk factors, suggesting orthogonal information of the  
496 splenic axis of CAD; in particular, rs7036656 and rs11515 on the Chr9p21 locus, one of the  
497 strongest CAD loci whose mechanism remained unclear since its initial discovery in 2007, is  
498 identified in our study as associated with splenic texture changes, such as energy and run length  
499 non-uniformity.<sup>47</sup> These findings, together, shed light on novel mechanisms linking the spleen to  
500 CAD, providing potential targets for therapeutic intervention to address this unexplored axis.

501 Our study has limitations. Firstly, the UK Biobank cohort includes participants of mostly  
502 European ancestry, and the participants were recruited between the ages of 40 and 59, limiting  
503 the generalizability of our findings to other ancestries and younger patients. These results should  
504 be replicated for a more diverse cohort. Second, we included participants whose MRI were  
505 categorized as “high-quality” by the segmentation model and filtered out “low-quality” ones

506 where the spleen was not identified. However, those filtered images may contain unique  
507 information that resulted in the classification. Third, to increase discovery power, we used a  
508 more liberal CAD definition, and therefore some associated splenic features may not be directly  
509 relevant to the etiology of strictly defined CAD.

510 In conclusion, by extracting novel splenic radiomics features linked to CAD and  
511 uncovering their genetic underpinnings, our work examined the unaddressed splenic axis of  
512 CAD. We demonstrated significant associations of splenic sphericity and texture variation with  
513 CAD risk, alongside identifying genetic variants and prioritizing genes tied to these spleen-CAD  
514 links. Leveraging several databases, we explored the functions of these genes and demonstrated  
515 their relevance and potential mechanisms to CAD etiology. Notably, we highlighted several loci,  
516 such as Chr9p21, linked to both splenic alterations and CAD yet unassociated with conventional  
517 CAD risk factors, presenting them as potential novel targets for therapeutic intervention.  
518 Together, our work presents a new framework to uncover the underexplored splenic axis of CAD.  
519

## 520 **Acknowledgments**

521 We gratefully acknowledge the participants who provided biological samples and data for UK  
522 Biobank. We also thank Mrs. Leslie Gaffney from the Broad Research Communication Lab for  
523 her valuable assistance in improving the display items.

524

## 525 **Funding**

526 P.L. receives funding support from the National Heart, Lung, and Blood Institute  
527 (1R01HL134892 and 1R01HL163099-01), the RRM Charitable Fund and the Simard Fund. P.N.  
528 is supported by grants from the NHLBI (R01HL142711, R01HL127564, R01HL148050,  
529 R01HL151283, R01HL148565, R01HL135242, and R01HL151152), National Institute of  
530 Diabetes and Digestive and Kidney Diseases (R01DK125782), Fondation Leducq (TNE-  
531 18CVD04), and Massachusetts General Hospital (Paul and Phyllis Fireman Endowed Chair in  
532 Vascular Medicine). R.B. is supported by Harvard Catalyst K12 Award. V.K.R. is supported by  
533 American Heart Association Career Development Award (935176). Z.Y. is supported by NHGRI  
534 (K99HG012956-01).

535

## 536 **Disclosures:**

537 A.P. is a General Partner at GV. P.L. is an unpaid consultant to, or involved in clinical trials for  
538 Amgen, AstraZeneca, Baim Institute, Beren Therapeutics, Esperion Therapeutics, Genentech,  
539 Kancera, Kowa Pharmaceuticals, Medimmune, Merck, Moderna, Novo Nordisk, Novartis, Pfizer,  
540 and Sanofi-Regeneron. P.L. is a member of the scientific advisory board for Amgen, Caristo  
541 Diagnostics, Cartesian Therapeutics, CSL Behring, DalCor Pharmaceuticals, Dewpoint  
542 Therapeutics, Eulucid Bioimaging, Kancera, Kowa Pharmaceuticals, Olatec Therapeutics,

543 Medimmune, Novartis, PlaqueTec, Polygon Therapeutics, TenSixteen Bio, Soley Thereapeutics,  
544 and XBiotech, Inc. P.L.'s laboratory has received research funding in the last 2 years from  
545 Novartis, Novo Nordisk and Genentech. P.L. is on the Board of Directors of XBiotech, Inc. P.L.  
546 has a financial interest in Xbiotech, a company developing therapeutic human antibodies, in  
547 TenSixteen Bio, a company targeting somatic mosaicism and clonal hematopoiesis of  
548 indeterminate potential (CHIP) to discover and develop novel therapeutics to treat age-related  
549 diseases, and in Soley Therapeutics, a biotechnology company that is combining artificial  
550 intelligence with molecular and cellular response detection for discovering and developing new  
551 drugs, currently focusing on cancer therapeutics. P.L.'s interests were reviewed and are managed  
552 by Brigham and Women's Hospital and Mass General Brigham in accordance with their conflict-  
553 of-interest policies. P.L. receives funding support from the National Heart, Lung, and Blood  
554 Institute (1R01HL134892, 1R01HL163099-01, R01AG063839, R01HL151627, R01HL157073,  
555 R01HL166538), the RRM Charitable Fund, and the Simard Fund. P.N. reports investigator-  
556 initiated grants from Amgen, Apple, Boston Scientific, Novartis, and AstraZeneca, personal fees  
557 from Allelica, Apple, AstraZeneca, Blackstone Life Sciences, Foresite Labs, Genentech, and  
558 Novartis, scientific board membership for Esperion Therapeutics, geneXwell, and TenSixteen  
559 Bio, and spousal employment at Vertex, all unrelated to the present work. P.N. is a scientific co-  
560 founders of TenSixteen Bio, and P.L. is an advisor to TenSixteen Bio. TenSixteen Bio is a  
561 company focused on clonal hematopoiesis but had no role in the present work. R.B. has been a  
562 advisor to Casana Care, Inc. unrelated to the current work. V.K.R has common stock in NVIDIA,  
563 Alphabet, Apple, and Meta. The other authors report no conflicts.

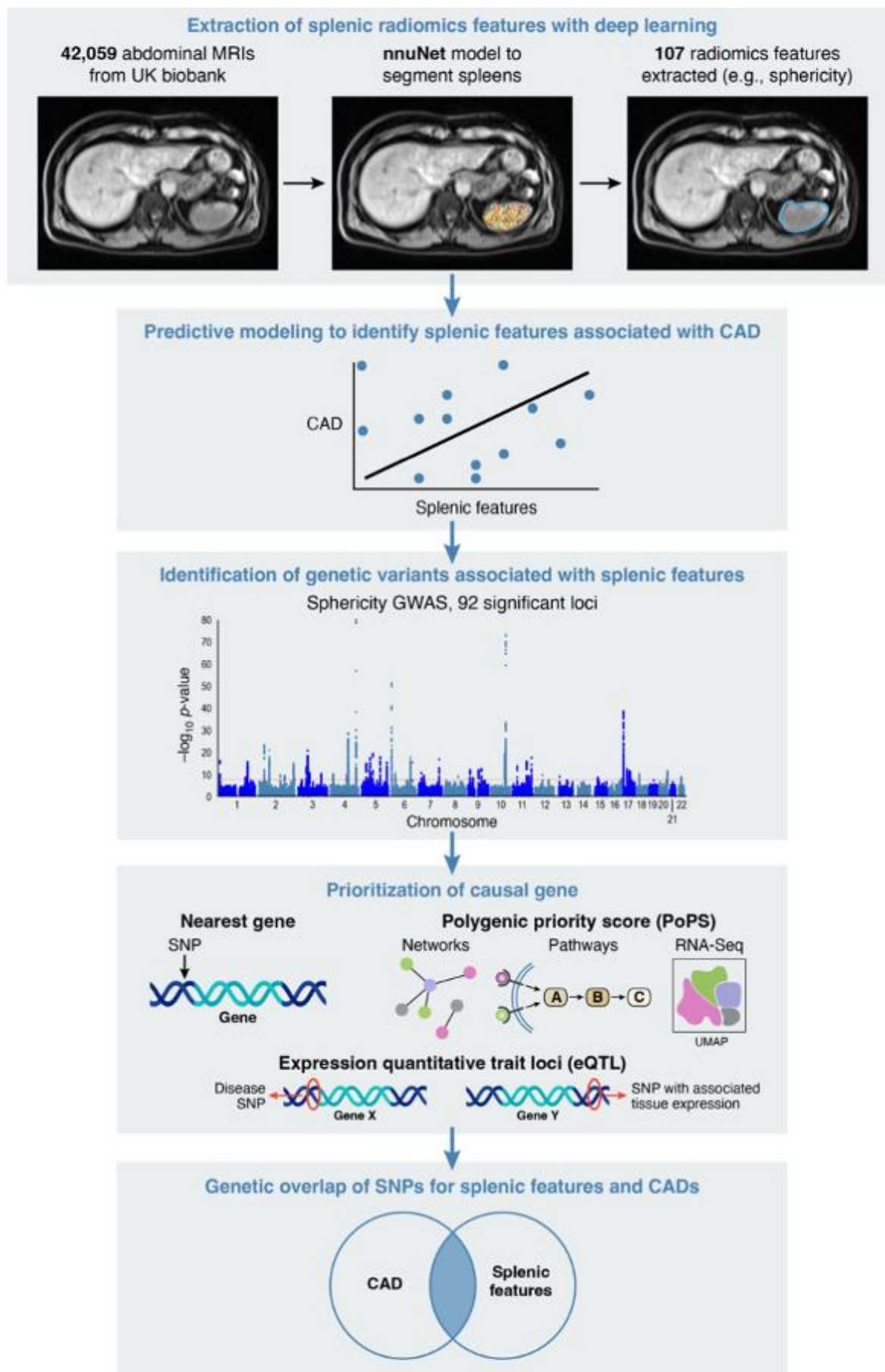
564 **Table 1. Baseline characteristics.** The number of incident and prevalent CAD cases in the  
565 cohort is shown below, and the gender and race breakdown of the population is also presented.  
566 For binary variables, metrics are represented as n (%). For continuous variables, age is  
567 represented as mean (SD), and all other continuous metrics are reported as median (IQR). All  
568 variables are measured at enrollment, unless an asterisk is included, indicating measurement at  
569 MRI date or, in the case of incident CAD, measurement at any point after MRI date. CAD,  
570 coronary artery disease. BMI, body-mass index. LDL, low-density lipoprotein. HDL, high-  
571 density lipoprotein. CAD, coronary artery disease. BMI, body mass index. LDL, low-density  
572 lipoprotein. HDL, high-density lipoprotein. \*measured at MRI date.

<b>Characteristic</b>	<b>Count or Mean (N=42,059)</b>
<b>Female</b>	21895 (52.1%)
<b>Age, years</b>	55.1 (7.5)
<b>British white ancestry</b>	40675 (96.7%)
<b>BMI, kg/m<sup>2</sup></b>	26.1 (23.7, 28.9)
<b>Systolic blood pressure, mmHg</b>	135.0 (124.0, 148.0)
<b>Diastolic blood pressure, mmHg</b>	81.0 (74.0, 88.0)
<b>Smoked ever</b>	12840 (30.5%)
<b>Alcohol intake frequency, drinks per week</b>	2.0 (2.0, 3.0)
<b>Total cholesterol, mmol/L</b>	4.58 (4.00, 5.17)
<b>LDL cholesterol, mmol/L</b>	3.54 (3.00, 4.11)
<b>HDL cholesterol, mmol/L</b>	1.43 (1.20, 1.70)
<b>Triglyceride, mmol/L</b>	1.40 (0.99, 2.02)
<b>Hyperlipidemia*</b>	7010 (16.7%)

<b>Type 2 diabetes*</b>	1243 (3.0%)
<b>Hypertension*</b>	10082 (24.0%)
<b>Prevalent CAD*</b>	1987 (4.7%)
<b>Incident CAD*</b>	993 (2.4%)

---

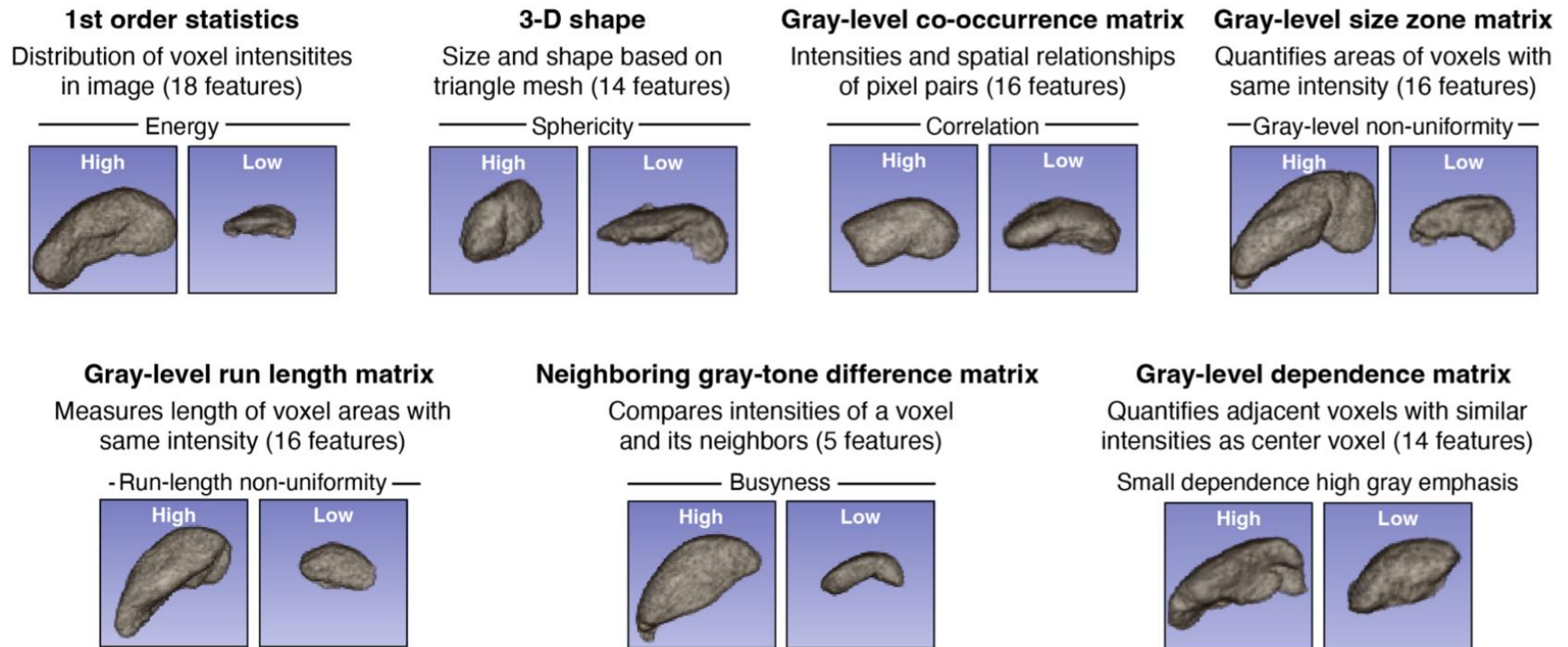
573



**nnuNet**: No New U-Net; **CAD**: coronary artery disease; **SNP**: single nucleotide polymorphism

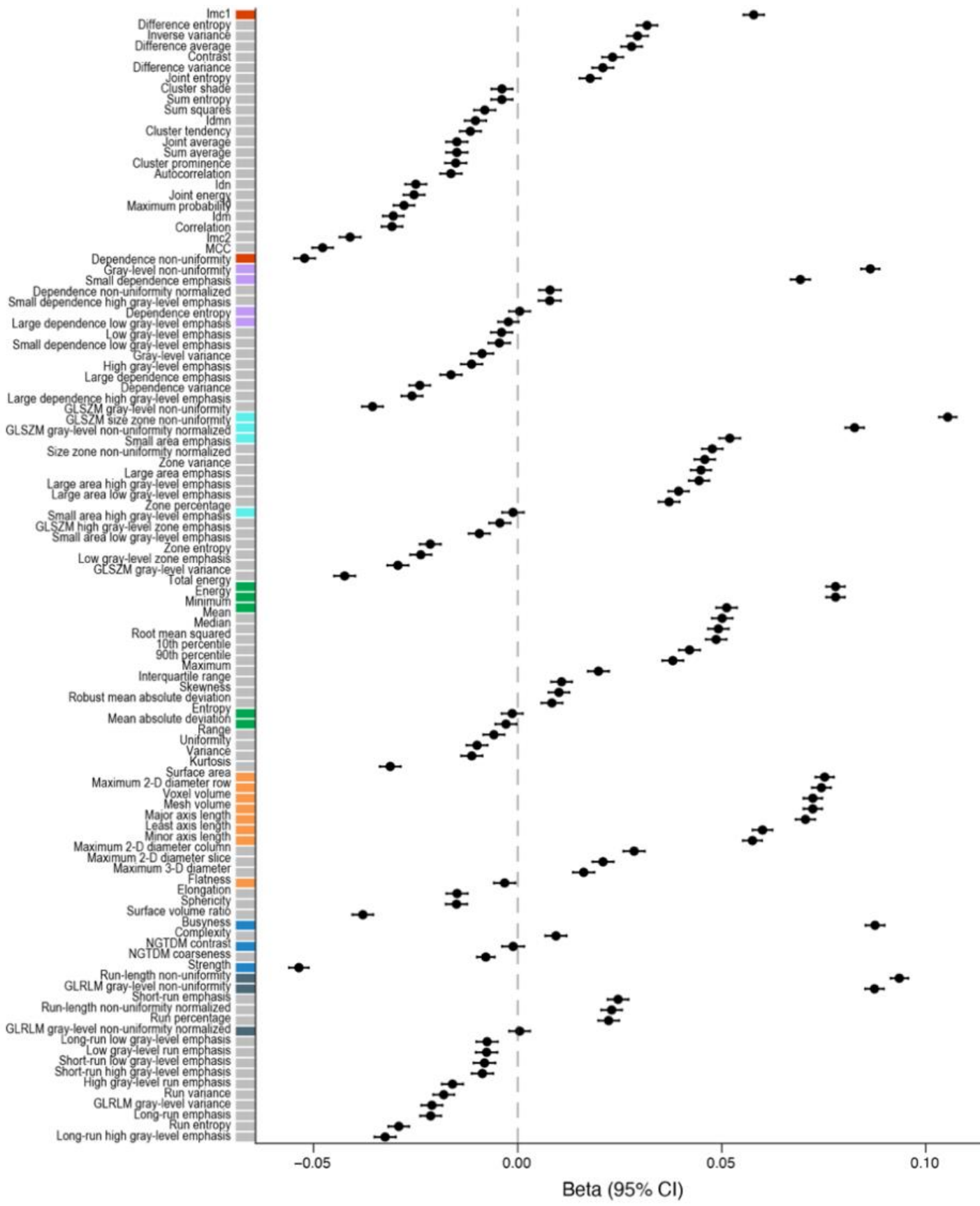
575 **Figure 1. Summary of the workflow to identify splenic features associated with CAD and**  
576 **discover genetic associations.** First, radiomics features describing the spleen are extracted from  
577 42,543 abdominal MRIs from the UK Biobank. Second, predictive models of each splenic  
578 radiomic feature for CAD are implemented. Genome-wide association studies are then conducted  
579 to identify genetic variants significantly associated with CAD-associated splenic radiomic  
580 features. Based on the identified genetic variants, genes are then prioritized for further  
581 investigation based on three different prioritization techniques: nearest gene, PoPS, and eQTL.  
582 Finally, the genetic variants that were associated with splenic radiomics were investigated for  
583 association with CAD using summary-level CAD GWAS meta-analysis. PoPs, polygenic priority  
584 score. eQTL, expression quantitative trait loci. nnuNet, No New U-Net. CAD, coronary artery  
585 disease. SNP, single nucleotide polymorphism. Reproduced by kind permission of UK Biobank  
586 ©.

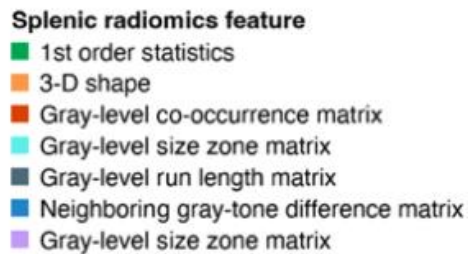




587

588 **Figure 2. Categorization of Extracted Splenic Radiomics Features.** 7 categories of radiomic features with descriptions, numbers of  
589 quantified features, and visualizations of high and low values for a selected feature. Reproduced by kind permission of UK Biobank ©.





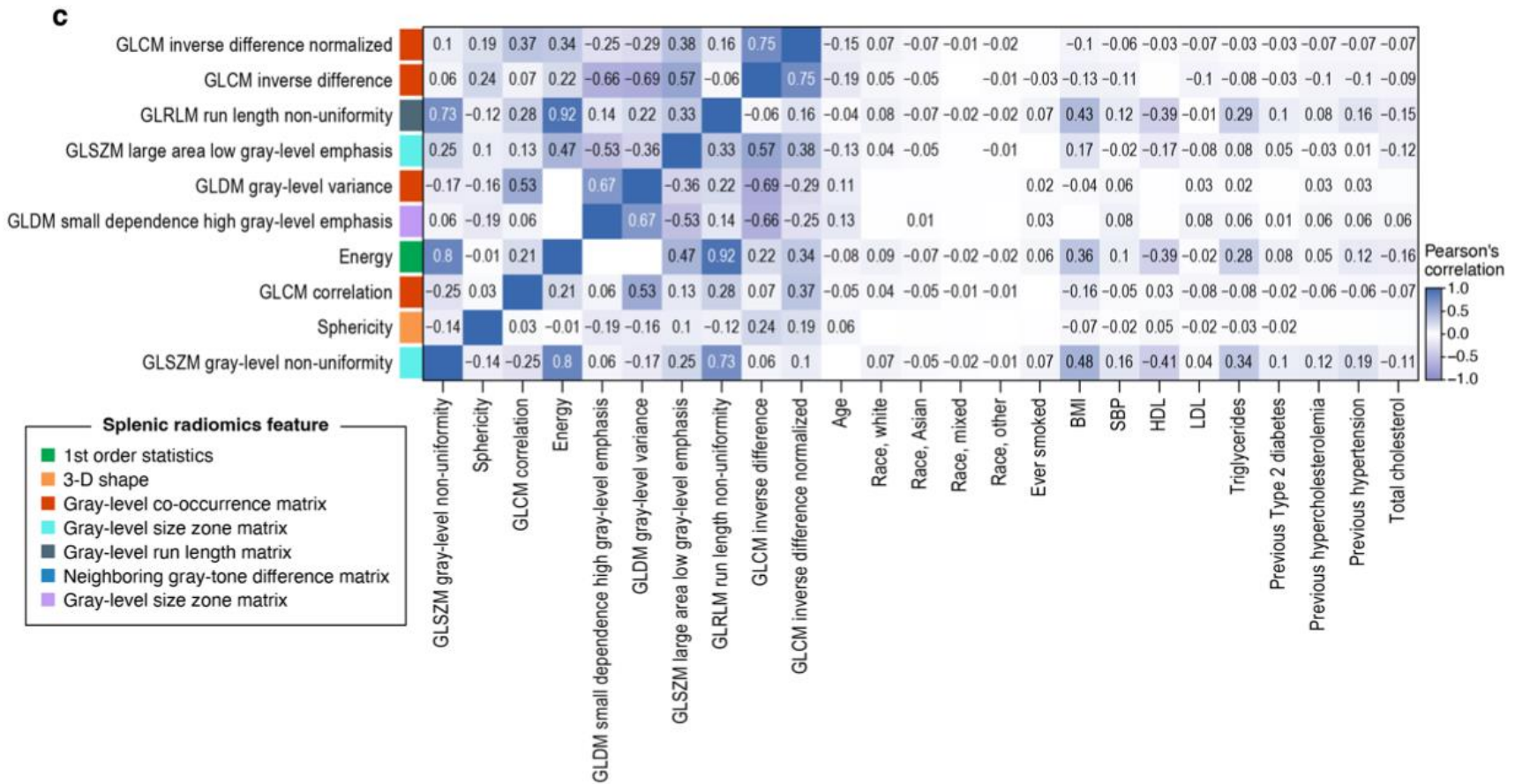
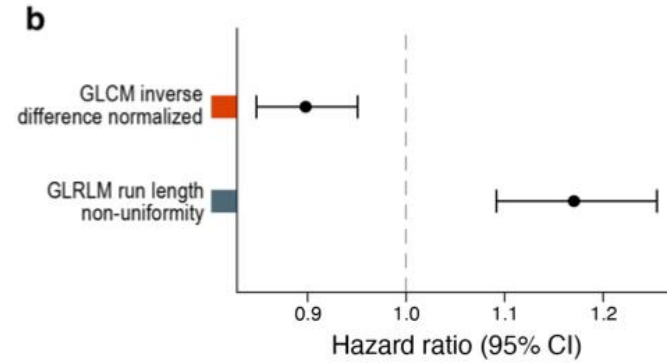
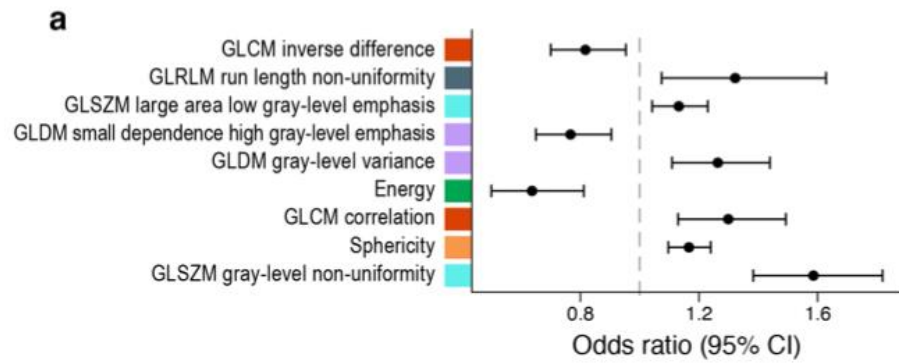
591

592 **Figure 3. Coefficients of BMI in a linear regression model for each splenic feature,**

593 **adjusting for age and sex.** Splenic radiomic features are grouped and colored by category using

594 the color scheme from Figure 2. Features are grayed out if the Bonferroni corrected p-value for

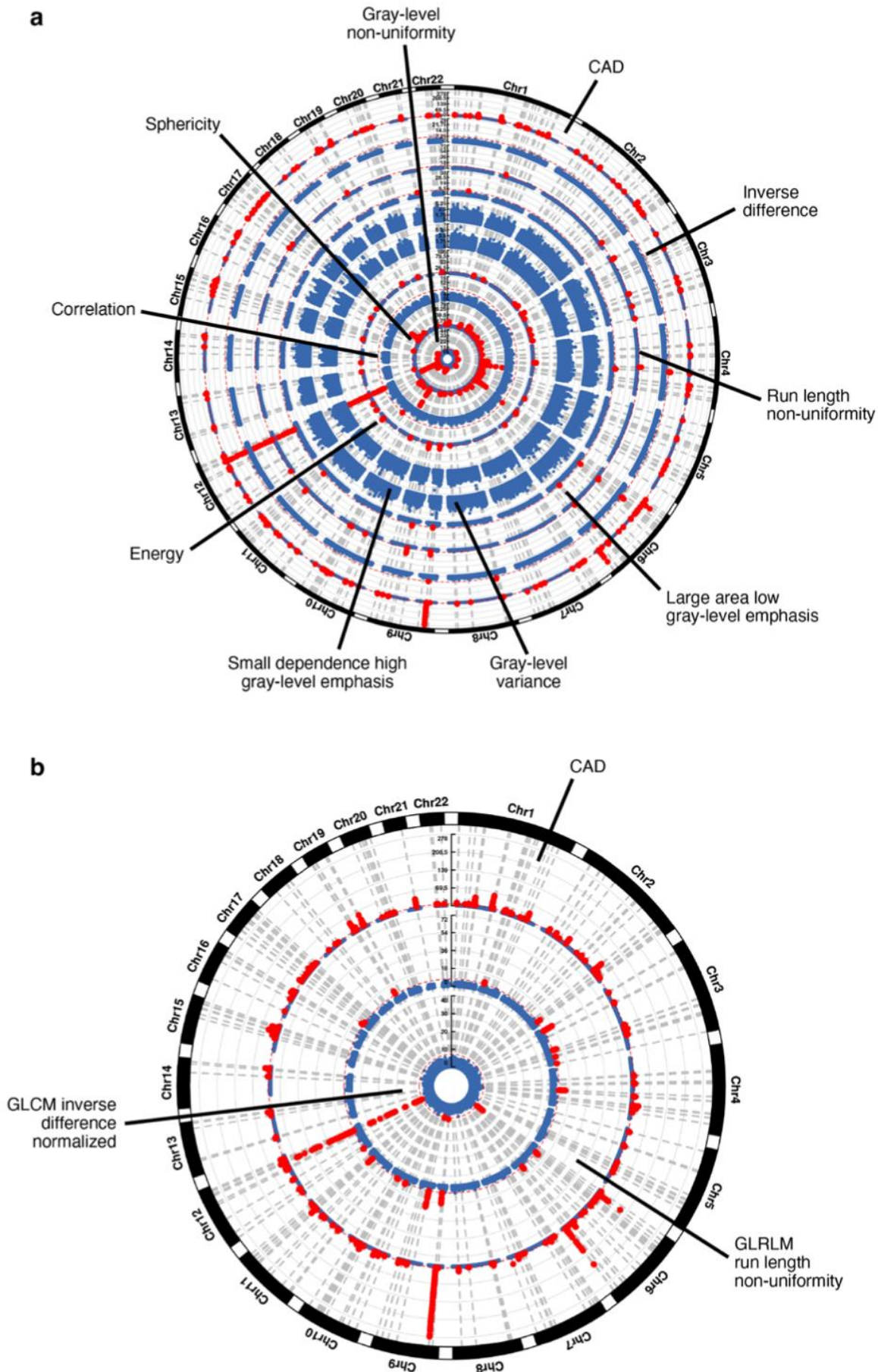
595 the coefficient of the BMI feature is greater than or equal to 0.05.



597 **Figure 4. Splenic radiomics features selected by prediction models for prevalent and incident CAD.** a) Splenic radiomics  
598 features that were nominally associated ( $p$ -value  $< 0.05$ ) with the prevalent CAD in a logistic regression model. b) Splenic radiomic  
599 features that were also nominally associated with incident CAD in a Cox regression survival analysis model among those without  
600 prevalent CAD. Covariates for both models included age, race, sex, and a set of splenic features chosen by forward stepwise  
601 regression, to ensure that no splenic features in the model were significantly correlated with each other. c) Correlations of the fourteen  
602 nominally significant splenic features across both models with conventional CAD risk factors. The Pearson correlation coefficient is  
603 shown for correlations that are significant.

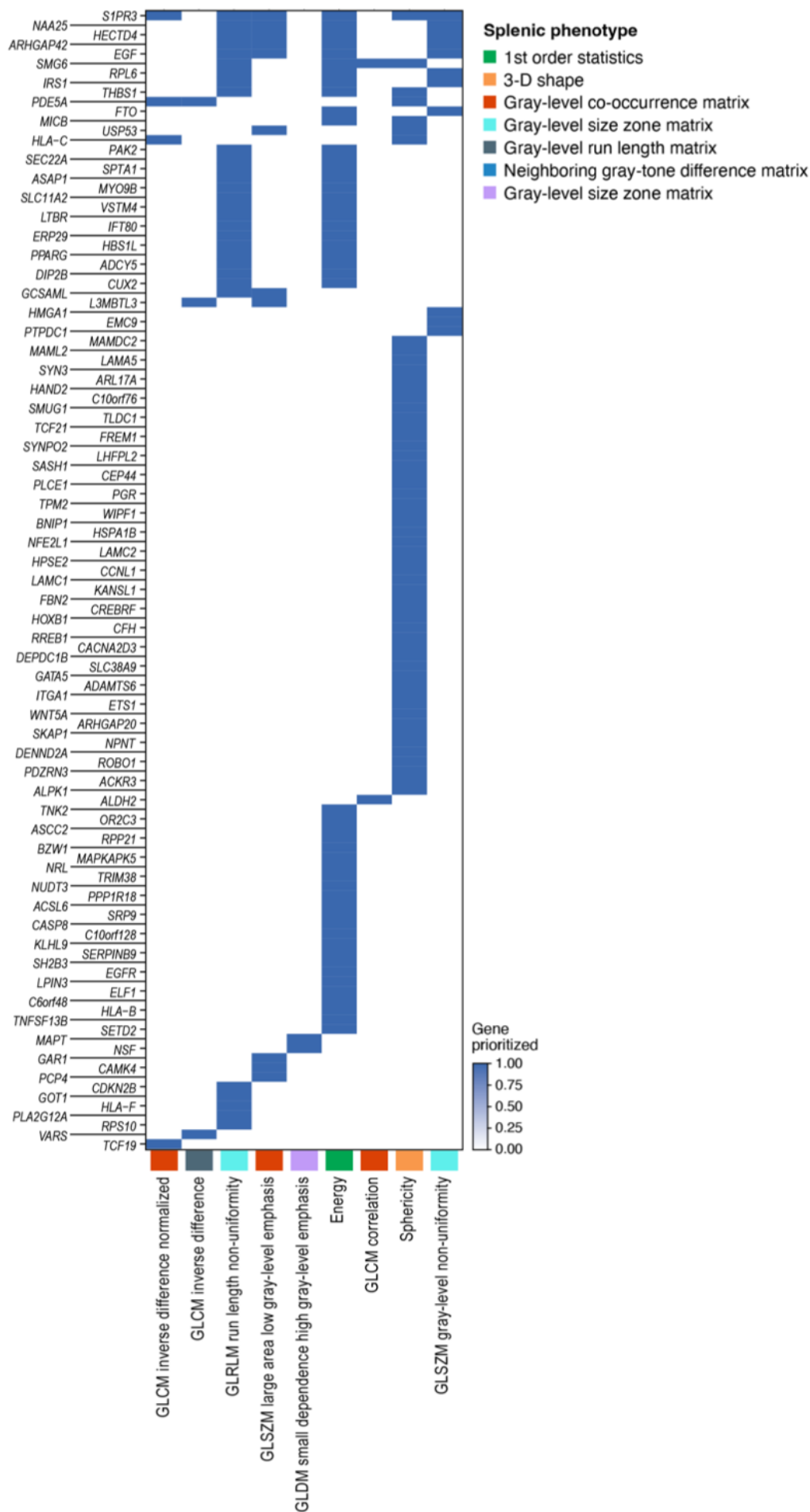
604 Higher gray non-uniform, gray level variance, and run-length non-uniformities values are associated with increased texture variation.  
605 Correlation refers to the correlation between voxel locations and their gray level intensities. A higher energy value indicates higher  
606 gray intensities. Higher small dependence high gray level emphasis indicates increased variation of areas of high gray levels. Higher  
607 large low gray level emphasis indicate decreased variation of areas of low gray levels respectively. Higher inverse difference reflects  
608 decreased texture variation of the spleen.

609 Feature abbreviations are as follows: Coronary Artery Disease, CAD. Energy, firstorder\_Energy. Sphericity, shape\_Sphericity.



611 **Figure 5. Circular Manhattan plots from GWAS with 14 splenic phenotypes and CAD. a)**

612 The circular Manhattan plot portrays the features that were statistically significant for prevalent  
613 CAD. From outside to inside, the features are CAD, GLCM inverse difference, GLRLM run  
614 length non-uniformity, GLSZM large area low gray level emphasis, GLDM gray level variance,  
615 GLDM small dependence high gray level emphasis, energy, GLCM correlation, sphericity, and  
616 GLSZM gray level-non uniformity. Red dots indicate significant loci. The y-axis is the log<sub>10</sub> of  
617 the p-value. b) The circular plot shows the features statistically significant for incident CAD.  
618 From outside to inside, the features are CAD, GLRLM run length non-uniformity, and GLCM  
619 inverse difference normalized. Feature abbreviations are as follows: CAD, Coronary Artery  
620 Disease. Correlation, glcm\_Correlation. Energy, firstorder\_Energy. Sphericity, shape\_Sphericity.





622 **Figure 6. Genes prioritized for CAD-associated splenic radiomics.** Genes were only included  
623 if they were prioritized by at least two methods (out of nearest gene, eQTL, PoPS) for at least  
624 one of the fourteen CAD-associated splenic phenotypes. Genes are grouped by the most  
625 associated splenic phenotypes from left to right. In addition, genes prioritized by similar  
626 phenotypes are grouped together.  
627 Feature abbreviations are as follows: Correlation, glcm\_Correlation. Energy, firstorder\_Energy.  
628 Sphericity, shape\_Sphericity.

## 629   **References**

- 630   1. Ralapanawa, U. & Sivakanesan, R. Epidemiology and the Magnitude of Coronary Artery  
631       Disease and Acute Coronary Syndrome: A Narrative Review: *J. Epidemiol. Glob. Health* **11**,  
632       169 (2021).
- 633   2. Vaduganathan, M., Mensah, G. A., Turco, J. V., Fuster, V. & Roth, G. A. The Global Burden  
634       of Cardiovascular Diseases and Risk. *J. Am. Coll. Cardiol.* **80**, 2361–2371 (2022).
- 635   3. Soehnlein, O. & Libby, P. Targeting inflammation in atherosclerosis — from experimental  
636       insights to the clinic. *Nat. Rev. Drug Discov.* **20**, 589–610 (2021).
- 637   4. Ridker, P. M. *et al.* Antiinflammatory Therapy with Canakinumab for Atherosclerotic  
638       Disease. *N. Engl. J. Med.* **377**, 1119–1131 (2017).
- 639   5. Yu, Z. *et al.* Genome-wide pleiotropy analysis of coronary artery disease and pneumonia  
640       identifies shared immune pathways. *Sci. Adv.* **8**, eab14602 (2022).
- 641   6. Heusch, G. The Spleen in Myocardial Infarction. *Circ. Res.* **124**, 26–28 (2019).
- 642   7. Dennis Robinette, C. & Fraumeni, Joseph F. SPLENECTOMY AND SUBSEQUENT  
643       MORTALITY IN VETERANS OF THE 1939-45 WAR. *The Lancet* **310**, 127–129 (1977).
- 644   8. Libby, P., Nahrendorf, M. & Swirski, F. K. Leukocytes Link Local and Systemic  
645       Inflammation in Ischemic Cardiovascular Disease. *J. Am. Coll. Cardiol.* **67**, 1091–1103  
646       (2016).
- 647   9. Dutta, P. *et al.* Myocardial infarction accelerates atherosclerosis. *Nature* **487**, 325–329 (2012).
- 648   10.    Van Der Laan, A. M. *et al.* Monocyte subset accumulation in the human heart following  
649       acute myocardial infarction and the role of the spleen as monocyte reservoir. *Eur. Heart J.* **35**,  
650       376–385 (2014).
- 651   11.    Emami, H. *et al.* Splenic Metabolic Activity Predicts Risk of Future Cardiovascular

- 652 Events. *JACC Cardiovasc. Imaging* **8**, 121–130 (2015).
- 653 12. Bon-Baret, V. *et al.* System Genetics Including Causal Inference Identify Immune  
654 Targets for Coronary Artery Disease and the Lifespan. *Circ. Genomic Precis. Med.* **14**,  
655 e003196 (2021).
- 656 13. Xu, P. *et al.* Radiomics: The Next Frontier of Cardiac Computed Tomography. *Circ.*  
657 *Cardiovasc. Imaging* **14**, e011747 (2021).
- 658 14. Enke, J. S. *et al.* Radiomics Features of the Spleen as Surrogates for CT-Based  
659 Lymphoma Diagnosis and Subtype Differentiation. *Cancers* **14**, 713 (2022).
- 660 15. Bycroft, C. *et al.* The UK Biobank resource with deep phenotyping and genomic data.  
661 *Nature* **562**, 203–209 (2018).
- 662 16. Honigberg, M. C. *et al.* Long-Term Cardiovascular Risk in Women With Hypertension  
663 During Pregnancy. *J. Am. Coll. Cardiol.* **74**, 2743–2754 (2019).
- 664 17. Littlejohns, T. J. *et al.* The UK Biobank imaging enhancement of 100,000 participants:  
665 rationale, data collection, management and future directions. *Nat. Commun.* **11**, 2624 (2020).
- 666 18. Kart, T. *et al.* Automated imaging-based abdominal organ segmentation and quality  
667 control in 20,000 participants of the UK Biobank and German National Cohort Studies. *Sci.*  
668 *Rep.* **12**, 18733 (2022).
- 669 19. Kart, T. *et al.* Deep Learning-Based Automated Abdominal Organ Segmentation in the  
670 UK Biobank and German National Cohort Magnetic Resonance Imaging Studies. *Invest.*  
671 *Radiol.* **56**, 401–408 (2021).
- 672 20. Gatidis, S. *et al.* Better Together: Data Harmonization and Cross-Study Analysis of  
673 Abdominal MRI Data From UK Biobank and the German National Cohort. *Invest. Radiol.* **58**,  
674 346–354 (2023).

- 675 21. van Griethuysen, J. J. M. *et al.* Computational Radiomics System to Decode the  
676 Radiographic Phenotype. *Cancer Res.* **77**, e104–e107 (2017).
- 677 22. Liu, Y. *et al.* Genetic architecture of 11 organ traits derived from abdominal MRI using  
678 deep learning. *eLife* **10**, e65554 (2021).
- 679 23. The 1000 Genomes Project Consortium *et al.* A global reference for human genetic  
680 variation. *Nature* **526**, 68–74 (2015).
- 681 24. Watanabe, K., Taskesen, E., Van Bochoven, A. & Posthuma, D. Functional mapping and  
682 annotation of genetic associations with FUMA. *Nat. Commun.* **8**, 1826 (2017).
- 683 25. Mountjoy, E. *et al.* An open approach to systematically prioritize causal variants and  
684 genes at all published human GWAS trait-associated loci. *Nat. Genet.* **53**, 1527–1533 (2021).
- 685 26. Weeks, E. M. *et al.* Leveraging polygenic enrichments of gene features to predict genes  
686 underlying complex traits and diseases. *Nat. Genet.* **55**, 1267–1276 (2023).
- 687 27. The International Mouse Phenotyping Consortium *et al.* High-throughput discovery of  
688 novel developmental phenotypes. *Nature* **537**, 508–514 (2016).
- 689 28. Groza, T. *et al.* The International Mouse Phenotyping Consortium: comprehensive  
690 knockout phenotyping underpinning the study of human disease. *Nucleic Acids Res.* **51**,  
691 D1038–D1045 (2023).
- 692 29. Aragam, K. G. *et al.* Discovery and systematic characterization of risk variants and genes  
693 for coronary artery disease in over a million participants. *Nat. Genet.* **54**, 1803–1815 (2022).
- 694 30. Fairley, S., Lowy-Gallego, E., Perry, E. & Flicek, P. The International Genome Sample  
695 Resource (IGSR) collection of open human genomic variation resources. *Nucleic Acids Res.*  
696 **48**, D941–D947 (2020).
- 697 31. Staley, J. R. *et al.* PhenoScanner: a database of human genotype-phenotype associations.

- 698 *Bioinforma. Oxf. Engl.* **32**, 3207–3209 (2016).
- 699 32. Kamat, M. A. *et al.* PhenoScanner V2: an expanded tool for searching human genotype-  
700 phenotype associations. *Bioinforma. Oxf. Engl.* **35**, 4851–4853 (2019).
- 701 33. Schizophrenia Working Group of the Psychiatric Genomics Consortium *et al.* LD Score  
702 regression distinguishes confounding from polygenicity in genome-wide association studies.  
703 *Nat. Genet.* **47**, 291–295 (2015).
- 704 34. Lavdas, I. *et al.* Machine learning in whole-body MRI: experiences and challenges from  
705 an applied study using multicentre data. *Clin. Radiol.* **74**, 346–356 (2019).
- 706 35. Lorensen, W. E. & Cline, H. E. Marching cubes: A high resolution 3D surface  
707 construction algorithm. in *Proceedings of the 14th annual conference on Computer graphics*  
708 *and interactive techniques* 163–169 (ACM, 1987). doi:10.1145/37401.37422.
- 709 36. Alaa, A. M., Bolton, T., Di Angelantonio, E., Rudd, J. H. F. & Van Der Schaar, M.  
710 Cardiovascular disease risk prediction using automated machine learning: A prospective study  
711 of 423,604 UK Biobank participants. *PLOS ONE* **14**, e0213653 (2019).
- 712 37. Zhuang, Y. *et al.* Circadian clocks are modulated by compartmentalized oscillating  
713 translation. *Cell* **186**, 3245-3260.e23 (2023).
- 714 38. Fjorder, A. S. *et al.* Haploinsufficiency of ARHGAP42 is associated with hypertension.  
715 *Eur. J. Hum. Genet.* **27**, 1296–1303 (2019).
- 716 39. Wafa, D. *et al.* Opposing Roles of S1P3 Receptors in Myocardial Function. *Cells* **9**, 1770  
717 (2020).
- 718 40. GTEx Consortium. Genetic effects on gene expression across human tissues. *Nature* **550**,  
719 204–213 (2017).
- 720 41. Mobeen Zafar, M. *et al.* 9p21 Locus Polymorphism Is A Strong Predictor of Metabolic

- 721 Syndrome and Cardiometabolic Risk Phenotypes Regardless of Coronary Heart Disease.  
722 *Genes* **13**, 2226 (2022).
- 723 42. Wellcome Trust Case Control Consortium *et al.* Genome-wide association study  
724 identifies eight loci associated with blood pressure. *Nat. Genet.* **41**, 666–676 (2009).
- 725 43. Vancauwenberghe, T., Snoeckx, A., Vanbeckevoort, D., Dymarkowski, S. &  
726 Vanhoenacker, F. Imaging of the spleen: what the clinician needs to know. *Singapore Med. J.*  
727 **56**, 133–144 (2015).
- 728 44. Zhang, X.-J. *et al.* Association between single nucleotide polymorphisms in  
729 thrombospondins genes and coronary artery disease: A meta-analysis. *Thromb. Res.* **136**, 45–  
730 51 (2015).
- 731 45. Dang, T. A. *et al.* Identification of a Functional *PDE5A* Variant at the Chromosome 4q27  
732 Coronary Artery Disease Locus in an Extended Myocardial Infarction Family. *Circulation*  
733 **144**, 662–665 (2021).
- 734 46. Nurnberg, S. T. *et al.* Coronary Artery Disease Associated Transcription Factor TCF21  
735 Regulates Smooth Muscle Precursor Cells That Contribute to the Fibrous Cap. *PLOS Genet.*  
736 **11**, e1005155 (2015).
- 737 47. Holdt, L. M. & Teupser, D. Recent Studies of the Human Chromosome 9p21 Locus,  
738 Which Is Associated With Atherosclerosis in Human Populations. *Arterioscler. Thromb. Vasc.*  
739 *Biol.* **32**, 196–206 (2012).